Acta Otolaryngol (Stockh) 1989; Suppl. 467: 265–279

CHAPTER 32

Nonlinear Dynamics of Cellular Vibrations in the Organ of Corti

MALVIN C. TEICH,[1] SHYAM M. KHANNA,[2] and SUZANNE E. KEILSON[1]

Columbia University, Departments of [1]Applied Physics and [2]Otolaryngology, New York, USA

INTRODUCTION

The motions of outer hair cells and Hensen's cells in the apical turn of the guinea pig cochlea (perpendicular to the reticular lamina) were previously measured in the isolated temporal bone preparation using heterodyne interferometry (Khanna, Flock and Ulfendahl, 1989, Khanna, Ulfendahl and Flock, 1989 a–e). The results of these experiments are analyzed in an attempt to gain understanding about the nature of the nonlinearity underlying their responses to acoustic stimulation. Displacement waveforms and their Fourier spectra, velocity waveforms and their spectra, and phase-space projections are provided for frequencies below, near, and above the frequency of maximum response. Plots of normalized velocity magnitude, as a function of signal frequency f_s, are provided for the first four harmonic components of the velocity spectrum. The two sets of data displayed here (one for an outer hair cell and one for a Hensen's cell) are representative of the 12 cells that have been analysed to date.

NUMERICAL PROCEDURE AND CONSTRUCTION OF PHASE-SPACE PROJECTIONS

Because the laser heterodyne interferometer operates on the basis of the Doppler effect (Willemin, Khanna and Dändliker, 1989), it provides a direct measurement of the instantaneous velocity of the cell in a direction parallel to that of the incident light. The data reported here were recorded in the form of 50 superposed repetitions of the velocity waveform (each of which was of duration 0.041 seconds). The signal was applied for 0.205 seconds before data collection was initiated. Details of the data collection procedures have been described earlier (Lund and Khanna, 1989).

The averaged velocity data sets were integrated in stepwise fashion to obtain discrete displacement waveforms,

$$x_i = \sum_{j=1}^{i} v_j \Delta t, \quad 1 \leq i \leq N; \; j \leq i \tag{1}$$

where v_j is the velocity recorded in the jth time interval, x_i is the displacement at the end of the ith time interval and Δt is the time resolution of the system or bin duration (10 microseconds in this set of experiments). N is the total number of time intervals or bins (4096), each of duration 10 microseconds, so that the total time duration was 0.041 seconds as indicated above. The result in Eq. (1) represents a kind of average displacement since it is obtained from averaged velocity waveforms.

Displacement and velocity values for the same time interval (bin) were then plotted on displacement versus velocity coordinates. This phase-space projection contains all of the

information related to the motion of the system with time eliminated as an explicit variable. Pure sinusoidal motion traces out an elliptical phase-space projection. This representation highlights deviations from sinusoidal behavior and phase differences between displacement and velocity.

Two initial conditions are required to calculate the absolute values of the displacement, but neither the initial displacement nor the initial velocity were experimentally determined. Furthermore, the mean velocity was not measured. We imposed a constraint on the calculation requiring that the mean velocity after an integer number of cycles of the sinusoidal signal be zero so that the final net displacement is also zero. The velocity zero was determined by integrating the velocity

$$C = \sum_{j=1}^{N} v_j \tag{2}$$

so that the incremental displacements were computed from

$$x_i = \sum_{j=1}^{i} (v_j - C/N)\,\Delta t, \quad 1 \leqslant i \leqslant N;\ j \leqslant i \tag{3}$$

where v_j, x_i, and N are defined the same way as in Eq. (1). We arbitrarily set x_o (the position at the time of the first velocity measurement) equal to zero. The quantity x_o is to be distinquished from $x(0) \equiv x(t=0)$, which is the initial displacement prior to the application of a signal. The unknown value of x_o results in an unknown constant added to each value of the displacement. Thus all displacement values shown in the figures should be viewed as relative displacements inasmuch as they are correct only to within an additive constant. It is not possible to impose a constraint on the mean displacement similar to that used for the mean velocity because the signal will, in general, result in an offset of the mean oscillator displacement from zero. Furthermore, the mean may fluctuate.

EXPERIMENTAL RESULTS

Outer hair cell

Data for an outer hair cell (7B131041), are presented in Figures 1–5. This cell has a best frequency of about 220 Hz. In Figures 1–4, results are shown in the form of (a) displacement waveforms, (b) displacement-waveform Fourier spectra, (c) velocity waveforms, (d) velocity-waveform Fourier spectra, and (e) phase-space projections. To avoid emphasizing the arbitrary displacement scale, the displacement axes in parts (a) and (e) of the figures are not drawn symmetrically about zero, as they were in our theoretical calculations (Keilson, Teich and Khanna, 1989 a, b; Teich, Keilson and Khanna, 1989 b). Figure 1 shows data at f_s=171 Hz, below the best frequency (CF); Figure 2 shows data at f_s=317 Hz, slightly above CF; Figures 3 and 4 show data well above CF, at f_s=610 and 806 Hz, respectively.

Examining the displacement waveforms at the four frequencies indicates that they appear to take the form of a quasi-sinusoidal waveform at the signal frequency added to a low-frequency randomly fluctuating waveform. The deviation of the signal frequency portion of the waveform from sinusoidal behavior is greatest below CF and decreases as the signal frequency increases. This is clear from the number of signal harmonic components present in the displacement spectra; the number is largest below CF and decreases as the signal frequency increases. The low-frequency fluctuation portion of the displacement waveform, on the other hand, increases in prominence with increasing signal

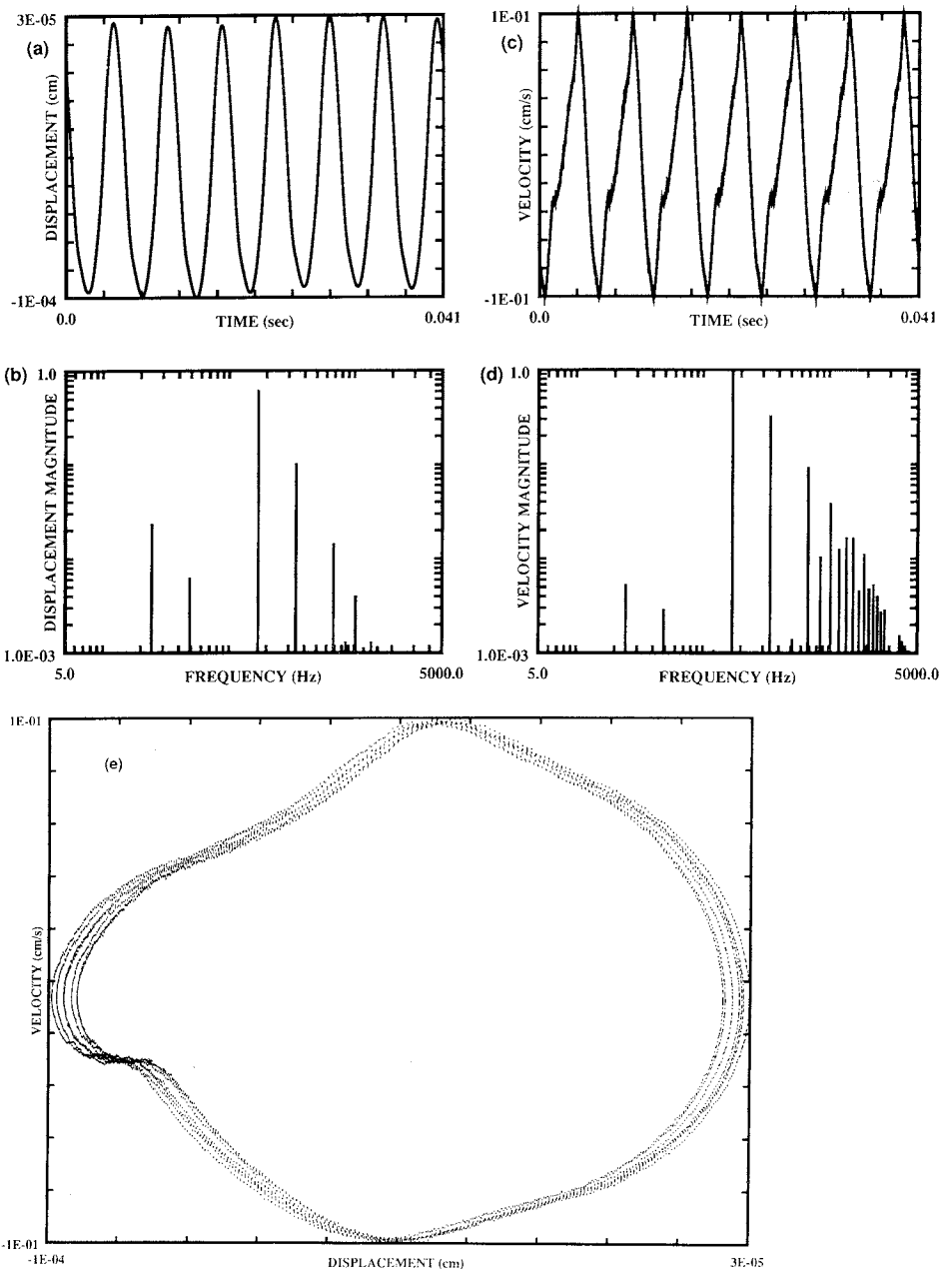

Fig. 1. Response of an outer hair cell in the guinea-pig cochlea (7B131041; CF=220 Hz) to a signal frequency f_s=171 Hz. (a) Time waveform of the displacement (the ordinate is determined only to within an additive constant). The response is nonsinusoidal. (b) Fourier spectrum of the displacement waveform. The signal frequency, three of its harmonics, and two anharmonic components are visible. (c) Time waveform of the velocity. The waveform is distorted from sinusoidal behavior. (d) Fourier spectrum of the velocity waveform. The velocity, being the derivative of the displacement, exhibits a greater number of high-frequency components. (e) Phase-space projection. The trace is distinctly non-elliptical and asymmetric.

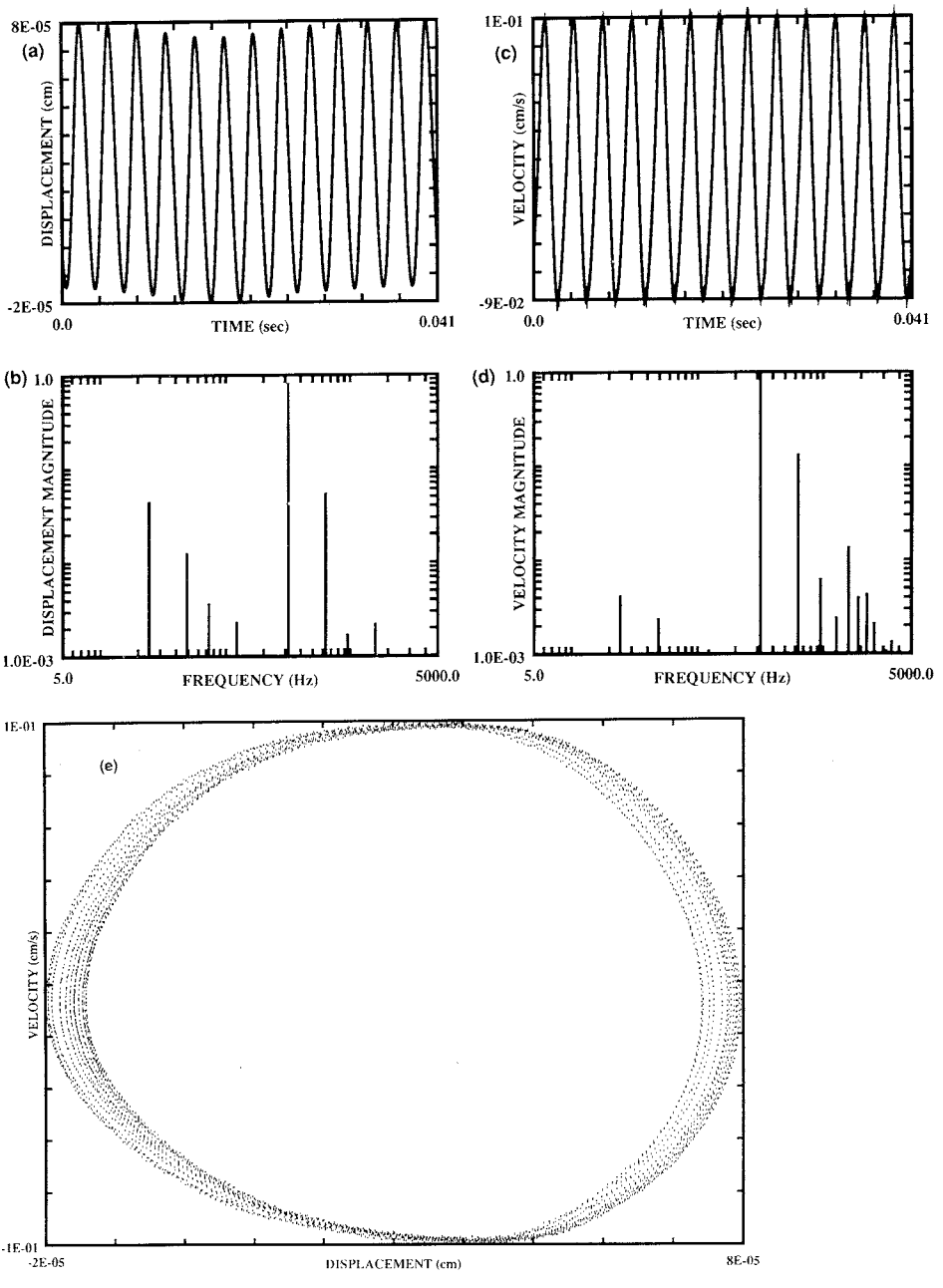

Fig. 2. Response of an outer hair cell in the guinea-pig cochlea (7B131041; CF=220 Hz) to a signal frequency f_s=317 Hz. (a) Time waveform of the displacement. The quasi-sinusoidal waveform appears to be riding on a low-frequency component. (b) Fourier spectrum of the displacement waveform. Although three harmonics are readily seen, only the second harmonic is comparable in relative value to that seen at 171 Hz in Figure 1(b). Four spectral components below 317 Hz are also visible. (c) Time waveform of the velocity. (d) Fourier spectrum of the velocity waveform. The number of high-frequency harmonics is greater than in the displacement spectrum. (e) Phase-space projection. The trace does not repeat itself on successive cycles; rather it slowly drifts back and forth as can be seen on the computer screen as it is being formed.

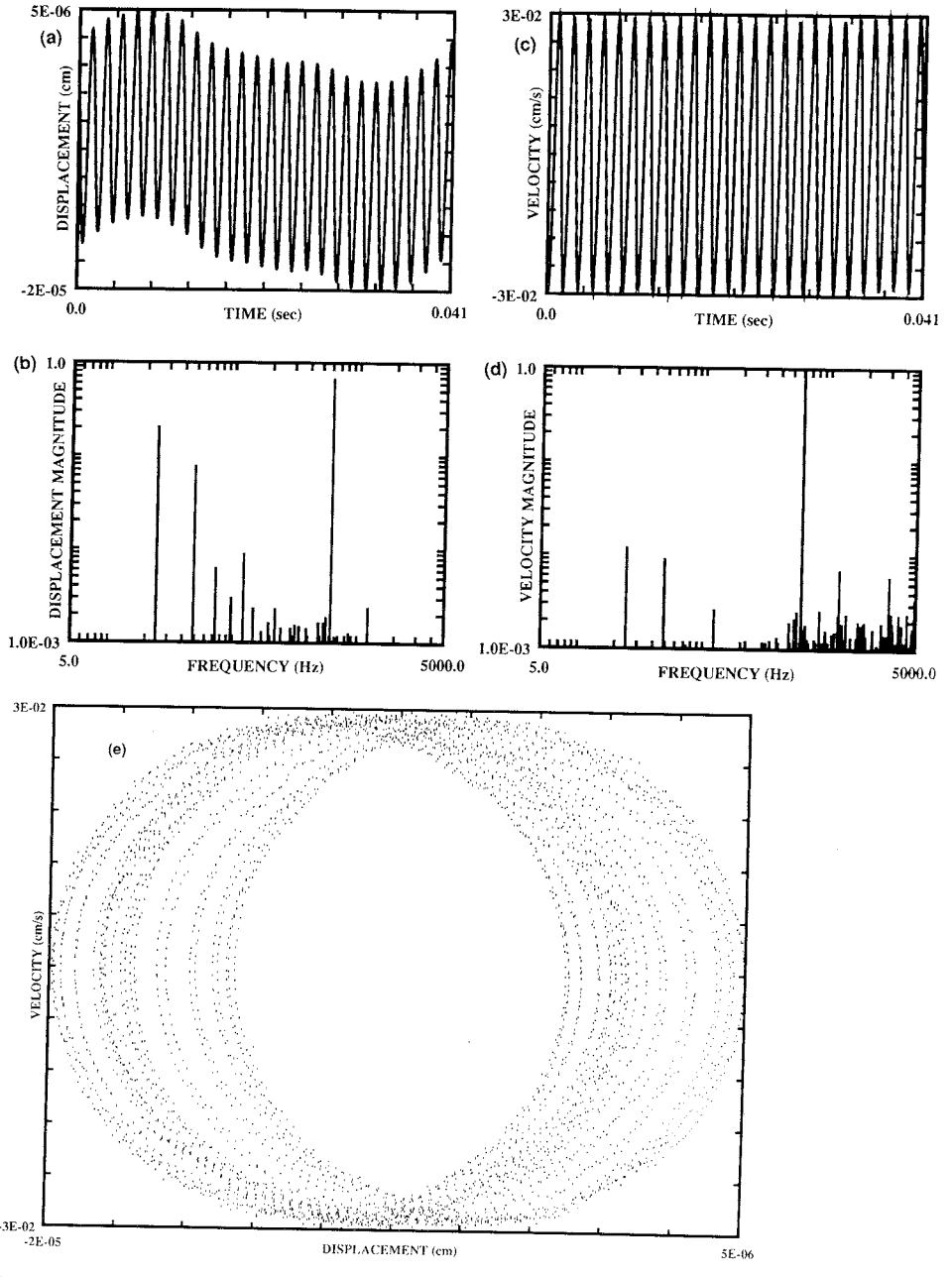

Fig. 3. Response of an outer hair cell in the guinea-pig cochlea (7B131041; CF=220 Hz) to a signal frequency f_s=610 Hz. (a) Time waveform of the displacement. The component of the waveform at the signal frequency is nearly sinusoidal, however the low-frequency aperiodic component is stronger than at lower signal frequencies. (b) Fourier spectrum of the displacement waveform. Only two harmonics of the signal frequency are readily seen, but a strong spectrum is evident below the signal frequency. (c) Time waveform of the velocity, which is rather sinusoidal. (d) Fourier spectrum of the velocity waveform. Two harmonics are visible above a quasi-continuous high frequency background. (e) Phase-space projection. The trace reveals large fluctuations in the displacement.

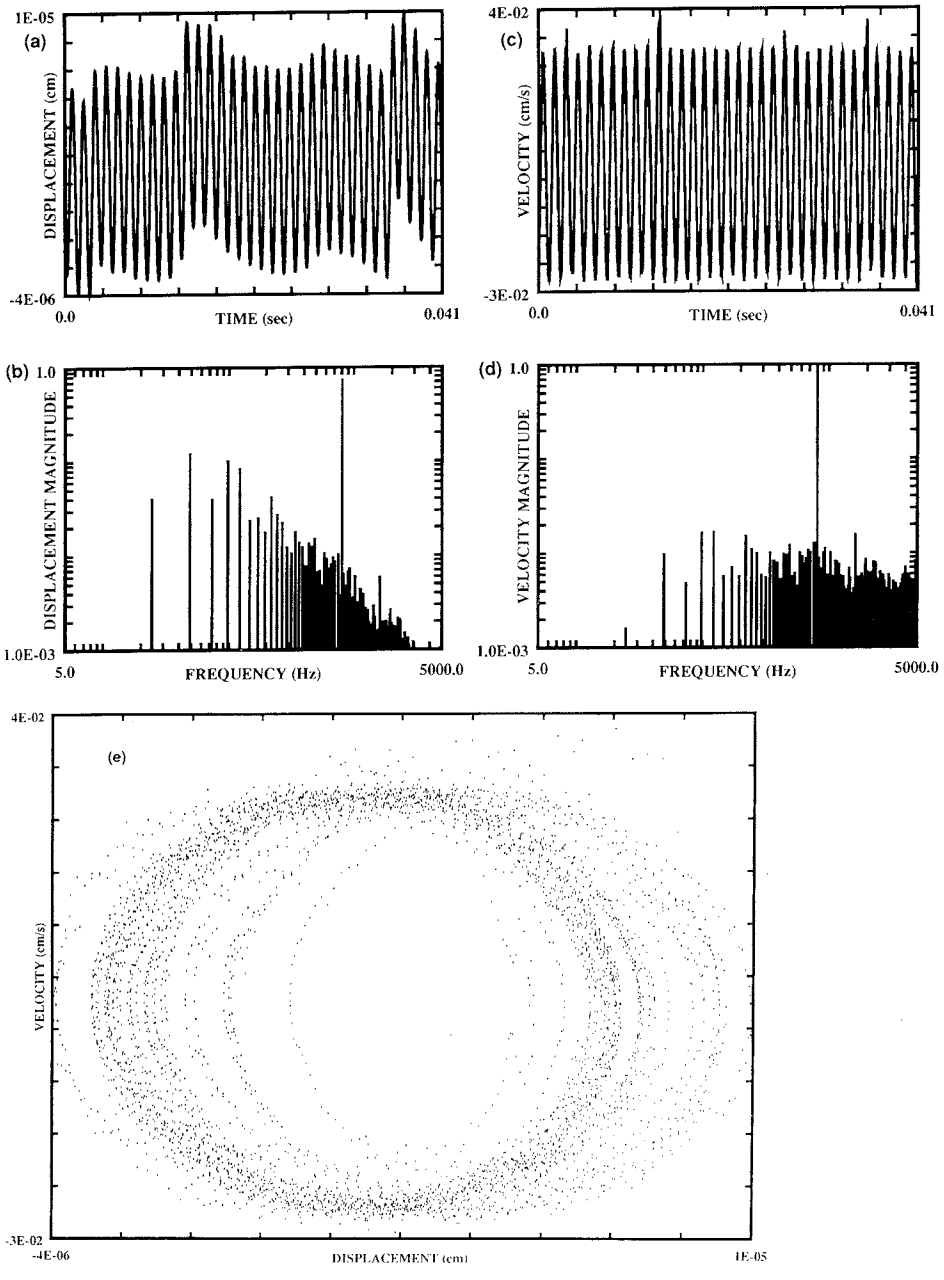

Fig. 4. Response of an outer hair cell in the guinea-pig cochlea (7B131041; CF=220 Hz) to a signal frequency f_s=806 Hz. (a) Time waveform of the displacement. Nonrepetitive jumps in the heights of successive cycles are evident. (b) Fourier spectrum of the displacement waveform. The low-frequency portion of the spectrum is 1/f-like. The component at the signal frequency is much larger than the background. (c) Time waveform of the velocity. Because the velocity is the derivative of the displacement, it deemphasizes the low-frequency jumps that are so clearly evident in the displacement waveform. (d) Fourier spectrum of the velocity waveform. As expected, the 1/f portion of the displacement spectrum is manifested as a constant level in the velocity spectrum. Only the fundamental stands distinctly above this level. (e) Phase-space projection. Successive traces fail to overlap, manifesting the presence of low-frequency aperiodic fluctuations.

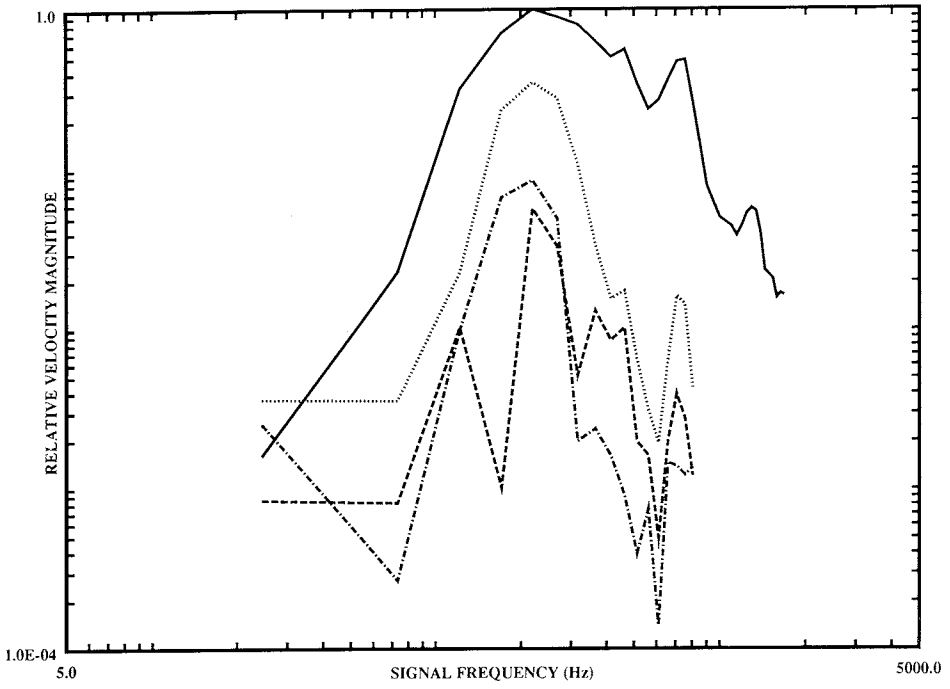

Fig. 5. Relative velocity-magnitude frequency-response curves (tuning curves) for an outer hair cell in the guinea-pig cochlea (7B131041; CF=220 Hz). The curves represent the magnitudes of the first four velocity harmonics, plotted as a function of the applied signal frequency. The curves are coded as follows: fundamental (solid curve), 2nd harmonic (dotted curved), 3rd harmonic (dashed curve), 4th harmonic (dash-dot curve). Multiple peaks are evident in the curves.

frequency. Correspondingly, the numbers and magnitudes of the low-frequency spectral components present in the displacement increase with increasing signal frequency.

Below CF, the deviations of the velocity waveforms from sinusoidal behavior are more pronounced than those of the displacement waveforms. These deviations decrease as the signal frequency increases. The low-frequency fluctuations present in the velocity waveforms, on the other hand, are less pronounced than those in the displacement waveforms. This is because the velocity is the derivative of the displacement and therefore emphasizes high frequency spectral components. The velocity spectra follow the same trend as the displacement spectra with increasing signal frequency.

The phase-space projections evidence nonelliptical and asymmetric behavior at all signal frequencies. Below CF, there is an indentation of the trace in some quadrants and small departures from overlap of the successive cycles traced out. These departures from overlap become more dramatic with increasing signal frequency and are a manifestation of the low-frequency anharmonic components of the motion. When traced out on the computer screen, the phase-space projection in Figure 3(e) reveals a rather slow and aperiodic motion that is quite evident in the displacement and velocity waveforms in Figures 3(a) and 3(c). Because this low frequency variation is aperiodic with respect to the sampling frequency, the discrete Fourier transform (DFT) routine treats the entire irregular waveform as a single cycle, whose fundamental is at the minimum allowable digital frequency (24 Hz), and thereby displays components at all of its multiples. The results shown in Figure 4, at f_s=806 Hz, are similar but even more dramatic.

The observed aperiodic low-frequency fluctuations, which become more pronounced as

the signal frequency increases, are not artifacts of the experimental measurement procedure; indeed these fluctuations are present in all of the cells that we have examined to date. This is in spite of the fact that the signal frequency portions of the velocity and displacement waveforms become ever more sinusoidal as the signal frequency increases. Another important feature of the experimental results is that, for high signal frequencies, the low-frequency portion of the Fourier transform of the displacement-waveform often takes the form of a 1/f-type spectrum, indicating the possibility of chaotic dynamics. The corresponding low-frequency continuous velocity spectrum is flat.

The relative magnitudes of the first four velocity harmonics are shown as a function of signal frequency in Figure 5. The first harmonic (fundamental) displays tuning, exhibiting a monotonic increase below the best frequency (~220 Hz), but rather unusual behavior above it. In particular there are sub-peaks at about 460 Hz, 750 Hz, and 1200 Hz. The shape of the velocity tuning observed at the fundamental frequency is quite different from that observed at the second, third, and fourth harmonics. Nevertheless, the frequencies of maximal response (best frequencies) of the higher harmonics are close to that of the fundamental; furthermore, they also exhibit multiple irregular peaks for signal frequencies above CF.

Hensen's cell

Figures 6–10 illustrate the results at selected frequencies for a Hensen's cell (7B131114). This cell also has a best frequency of about 220 Hz. In Figures 6–9, results are shown in the form of (a) displacement waveforms, (b) displacement-waveform Fourier spectra, (c) velocity waveforms, (d) velocity-waveform Fourier spectra, and (e) phase-space projections. Again, the displacement axes in parts (a) and (e) are not drawn symmetrically to avoid emphasizing the arbitrary displacement scale. Figure 6 shows data at $f_s=171$ Hz, below the CF; Figure 7 shows data at $f_s=317$ Hz, slightly above CF; Figures 8 and 9 show data well above CF, at $f_s=610$ and 806 Hz, respectively.

Examining the displacement waveforms at the four frequencies reveals quite similar behavior to that observed for the outer hair cell, as shown in Figures 1–4. The deviation of the signal-frequency portion of the waveform from sinusoidal behavior is greatest below CF and decreases as the signal frequency increases. Again, the number of signal harmonics present in the displacement spectra is greatest below CF and decreases as the signal frequency increases. The low-frequency fluctuation of the displacement waveform, on the other hand, increases in prominence with increasing signal frequency. Correspondingly, the numbers and magnitudes of the low-frequency spectral components present in the displacement increase with increasing signal frequency.

Below CF, the deviations of the velocity waveforms from sinusoidal behavior are more pronounced than those of the displacement waveforms. These deviations decrease as the signal frequency increases. The low-frequency fluctuations present in the velocity waveforms, on the other hand, are less pronounced than those in the displacement waveforms since the velocity is the derivative of the displacement. The velocity spectra follow the same trend as the displacement spectra with increasing signal frequency.

The phase-space projections evidence nonelliptical and asymmetric behavior at all signal frequencies. Below CF, the phase-space projection trace of Figure 6(e) reveals undulations with a frequency about 11 times that of the fundamental response (signal) frequency. The velocity spectrum shown in Figure 6(d), although somewhat dense, is composed primarily of higher harmonics of the signal frequency. Less symmetrical indentations were evident in the phase-space projection for the outer hair cell below CF, as shown in Figure 1(e). Departures from overlap of successive cycles, which are already

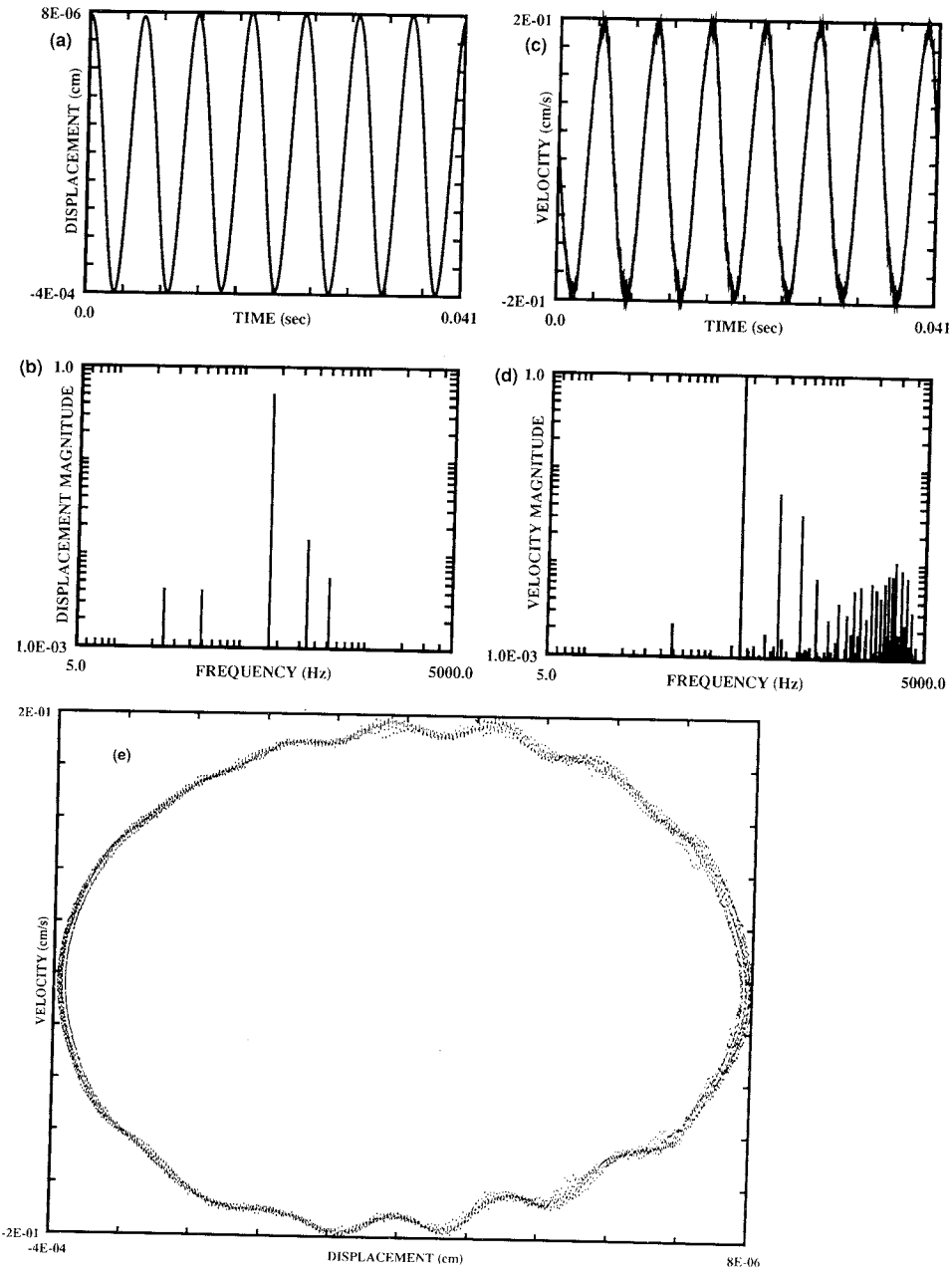

Fig. 6. Response of a Hensen's cell in the guinea-pig cochlea (7B131114; CF=220 Hz) to a signal frequency f_s=171 Hz. (a) Time waveform of the displacement (the ordinate is determined only to within an additive constant). The response is nonsinusoidal. (b) Fourier spectrum of the displacement waveform. Three harmonics and two anharmonic components below the signal frequency are visible. (c) Time waveform of the velocity. (d) Fourier spectrum of the velocity waveform. The velocity, being the derivative of the displacement, exhibits a greater number of high-frequency components. (e) Phase-space projection. The trace is distinctly non-elliptical and asymmetric for both positive and negative displacements and velocities. It shows high frequency undulations phase locked to the velocity waveform.

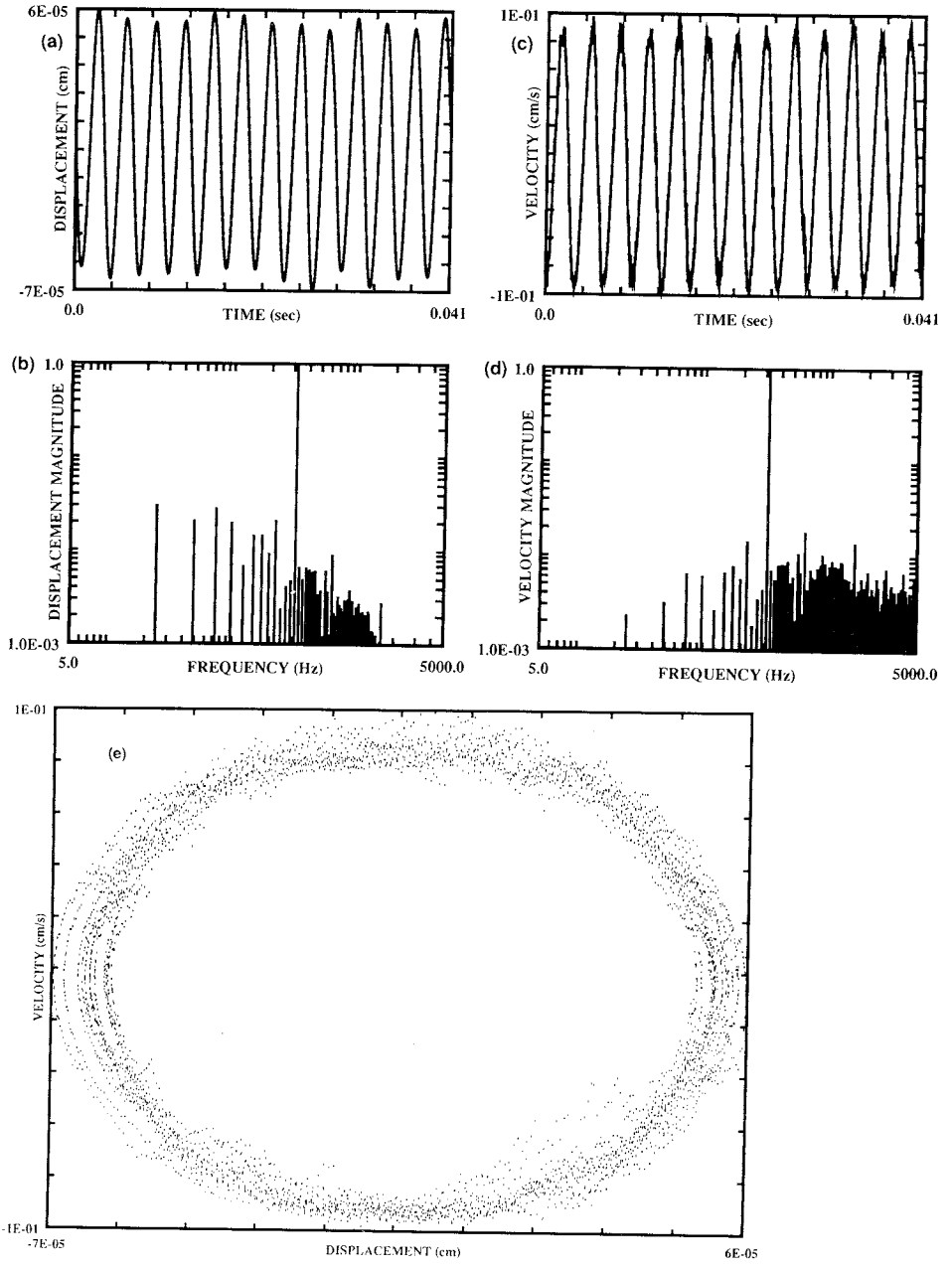

Fig. 7. Response of a Hensen's cell in the guinea-pig cochlea (7B131114; CF=220 Hz) to a signal frequency f_s=317 Hz. (a) Time waveform of the displacement. The rather sinusoidal waveform at the signal frequency appears to be riding on a low-frequency aperiodic waveform. (b) Fourier spectrum of the displacement waveform. The fundamental component stands above the continuous spectrum representing the aperiodic variations. (c) Time waveform of the velocity. (d) Fourier spectrum of the velocity waveform. The number of high-frequency harmonics is greater than that in the displacement spectrum. (e) Phase-space projection. The trace does not repeat itself on successive cycles; rather it slowly drifts back and forth.

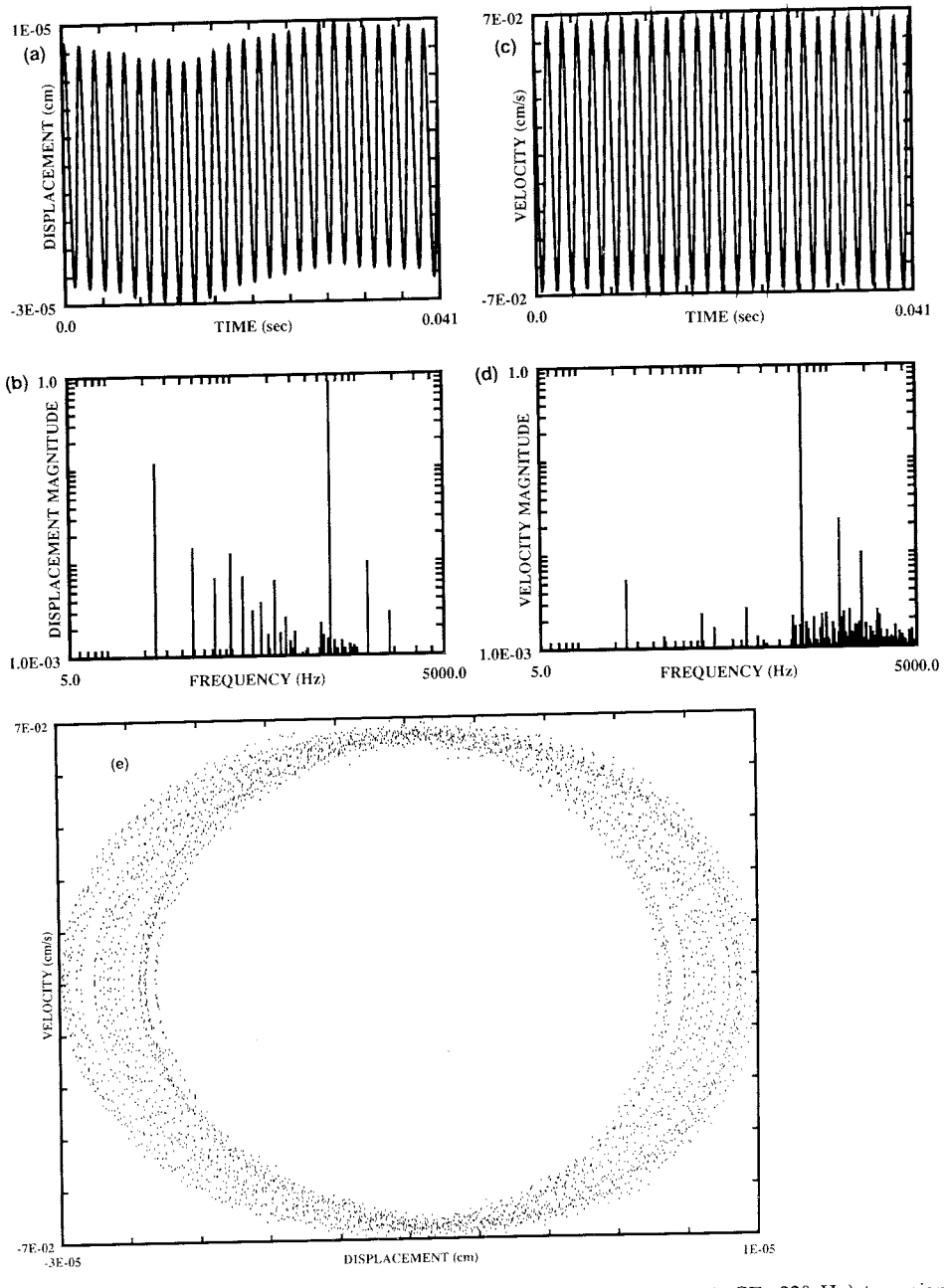

Fig. 8. Response of a Hensen's cell in the guinea-pig cochlea (7B131114; CF=220 Hz) to a signal frequency f_s=610 Hz. (a) Time waveform of the displacement. The waveform has a sinusoidal appearance but successive cycles of the waveform clearly exhibit aperiodic fluctuations. (b) Fourier spectrum of the displacement waveform. Only three harmonics of the signal are readily seen, but the continuous spectrum below the signal frequency is rather strong. (c) Time waveform of the velocity. Again, successive cycles of the waveform peaks display slight fluctuations. (d) Fourier spectrum of the velocity waveform. Three harmonics are visible above the background. (e) Phase-space projection. The trace reveals large fluctuations in the displacement.

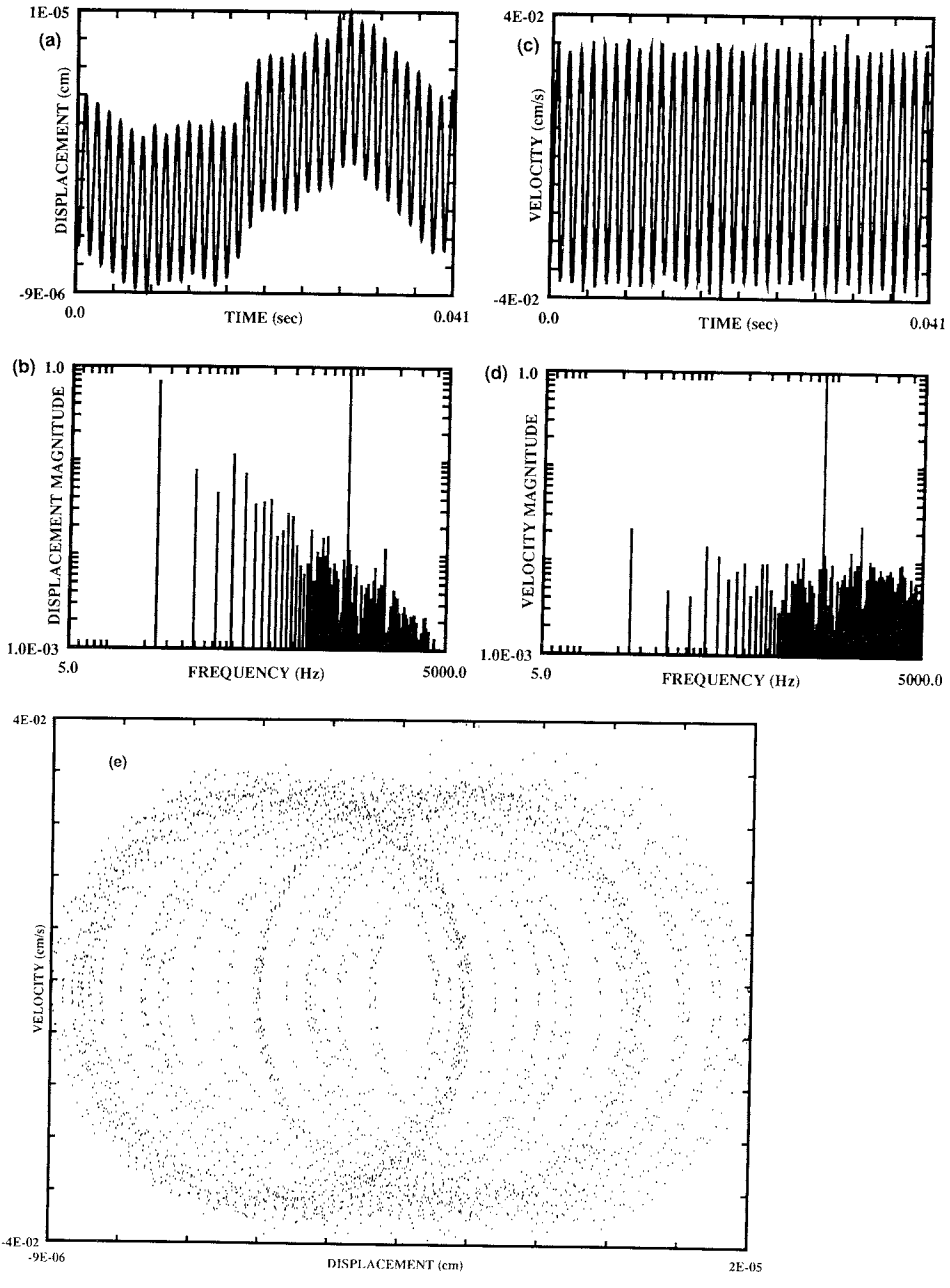

Fig. 9. Response of a Hensen's cell in the guinea-pig cochlea (7B131114; CF=220 Hz) to a signal frequency f_s=806 Hz. (a) Time waveform of the displacement. Nonrepetitive jumps in the heights of successive cycles are evident. (b) Fourier spectrum of the displacement waveform. The low-frequency portion of the spectrum is 1/f-like but the fundamental emerges above this. (c) Time waveform of the velocity. Because the velocity is the derivative of the displacement, it deemphasizes the low-frequency jumps that are so clearly evident in the displacement waveform. (d) Fourier spectrum of the velocity waveform. As expected, the 1/f portion of the displacement spectrum is reflected as a constant level in the velocity spectrum. Only the fundamental stands distinctly above this level. (e) Phase-space projection. The trace does not repeat itself and manifests slow but substantial aperiodic fluctuations.

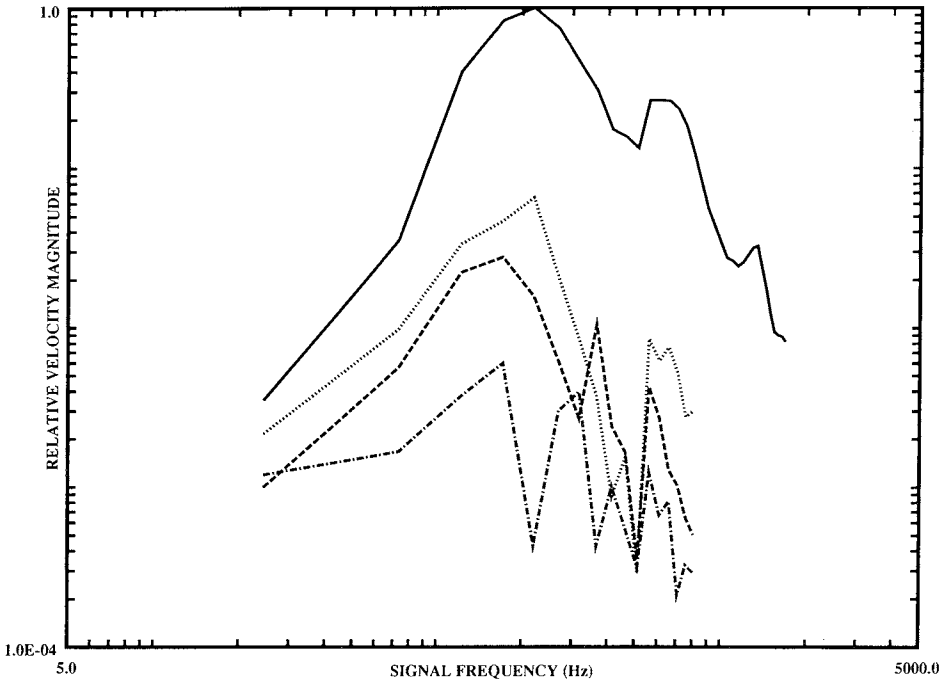

Fig. 10. Relative velocity-magnitude frequency-response curves (tuning curves) for the response of a Hensen's cell in the guinea-pig cochlea (7B131114; CF=220 Hz). The curves represent the magnitudes of the first four velocity harmonics, plotted as a function of the applied signal frequency. The curves are coded as follows: fundamental (solid curve), 2nd harmonic (dotted curved), 3rd harmonic (dashed curve), 4th harmonic (dash-dot curve). As in the case of the hair cell results shown in Figure 5, multiple peaks are evident in the curves.

evident in Figure 6(e), increase with increasing signal frequency and are a manifestation of the low-frequency anharmonic components of the motion. When these phase-space projections are traced out on the computer screen the underlying ellipsoidal response can be seen to slowly oscillate back and forth under the low-frequency fluctuations. The results are similar to those for the outer hair cell and indeed for all of the cells examined to date. For high signal frequencies, the low-frequency portion of the Fourier transform of the displacement-waveform again takes the form of a 1/f-type spectrum, as may be seen in Figures 8(b) and 9(b).

The first through fourth harmonics of the relative velocity magnitude are shown as a function of the applied signal frequency in Figure 10. Again, the fundamental curve displays tuning. Like the outer hair cell, the Hensen's cell shows monotonic behavior below the best frequency (~220 Hz), and secondary peaks above the best frequency, in this case at about 600 Hz and 1200 Hz. The higher harmonic tuning curves exhibit multiple, irregular peaks above the CF as well, at frequencies near those of the subpeaks in the fundamental tuning curve.

COMPARISON OF EXPERIMENTAL RESULTS WITH BILINEAR OSCILLATOR MODELS

We now proceed to compare the theoretical results obtained from the bilinear mass oscillator (Keilson, Teich and Khanna, 1989b), the bilinear stiffness oscillator (Teich,

Keilson and Khanna 1989b), and the bilinear resistance oscillator (Keilson, Teich and Khanna, 1989a) with this data. The cascade of a linear filter and a static rectifying element with arbitrary clipping level (Teich, Keilson and Khanna, 1989a), gives rise to results that are also in poor agreement with the data so that this model is not considered further here.

All three bilinear oscillator models can produce indentations in the phase-space projection at low signal frequencies, similar to those seen in Figure 1(e). In the realm in which we have examined them, none of the models gives rise to undulations in the phase-space projection and the associated high-frequency harmonic components, evident in Figure 6(e). The bilinear mass and the bilinear resistance models can give rise to low-frequency aperiodic fluctuations of the displacement and velocity, whereas the bilinear stiffness model cannot . The bilinear mass model leads to relative velocity magnitude curves (tuning curves) which resemble the data far more than do those of the bilinear stiffness or resistance models. In particular, the bilinear mass model tuning curves at the various harmonics exhibit multiple peaks and a strong subharmonic resonance (which was not experimentally sought, however).

In spite of their simplicity, all three of the bilinear models exhibit some of the features present in the data. Although the bilinear mass model is probably the best of the three in this regard, none of the models is entirely satisfactory for describing the cellular vibrations reported here. Nevertheless, these simple models provide a point of departure. Complex dynamics can be present in an exceptionally simple nonlinear system, thereby obviating the necessity for contrived nonlinearities and ad hoc signal processing schemes. A detailed study of where these simple models fail to account for the experimental results will be instructive for developing a more appropriate nonlinear model.

DISCUSSION

Phase-space projections eliminate time as an explicit variable; they highlight the deviations of nonlinear-system responses from sinusoidal behavior and the differences in phase between displacement and velocity. They are useful for emphasizing features of the data that are not readily apparent in time waveforms and spectra. Displacement waveforms emphasize low-frequency information (relative to velocity waveforms) because the former is the integral of the latter; velocity waveforms relatively emphasize high-frequency information. The Fourier transforms of both kinds of waveform reveal the presence of harmonics of the signal frequency, as well as aperiodic low-frequency components which appear as multiples of the fundamental digital sampling frequency (24 Hz).

The data from an outer hair cell and a Hensen's cell are remarkably similar. Four general features emerge from our analysis: (a) Deviations of the phase-space projection from ellipticity, indicating nonlinear behavior. These deviations take the form of indentations in various quadrants at signal frequencies below the best frequency; (b) Undulations in the phase-space projection associated with high-frequency fluctuations in the velocity waveform that are harmonically related and phase locked to the signal frequency, also below the CF; (c) Slowly oscillating phase-space projections associated with low-frequency aperiodic fluctuations of the displacement (and velocity), occurring at signal frequencies above the best frequency. For such signal frequencies, the spectrum of the displacement waveform at low frequencies behaves in a 1/f-like manner, suggesting the possibility of chaotic dynamics; (d) Harmonics of the velocity waveform that have decreasing relative magnitudes and peak near the same best frequency as the fundamental. These curves essentially increase monotonically below the best frequency, but exhibit multiple sub-peaks above it.

In closing we note that the apparent plethora of complex behavior observed in the cellular vibrations in the organ of Corti may well have a simple (nonlinear) underlying origin.

ACKNOWLEDGEMENTS

This work was supported by the National Institutes of Health and the National Science Foundation.

REFERENCES

Keilson SE, Teich MC, Khanna SM (1989a). Models of nonlinear vibration. I. Oscillator with bilinear resistance. Acta Otolaryngol (Stockh) Suppl 467: 241–248.

Keilson SE, Teich MC, Khanna SM (1989b). Models of nonlinear vibration. III. Oscillator with bilinear mass. Acta Otolaryngol (Stockh) Suppl 467: 257–264.

Khanna SM, Flock Å, Ulfendahl M (1989). Changes in cellular tuning along the radial axis of the cochlea. Acta Otolaryngol (Stockh) Suppl 467: 163–173.

Khanna SM, Ulfendahl M, Flock Å (1989a). Mechanical tuning characteristics of outer hair cells and Hensen's cells. Acta Otolaryngol (Stockh) Suppl 467: 139–144.

Khanna SM, Ulfendahl M, Flock Å (1989b). Changes in cellular tuning along the length of the cochlea. Acta Otolaryngol (Stockh) Suppl 467: 157–162.

Khanna SM, Ulfendahl M, Flock Å (1989c). Waveforms and spectra of cellular vibrations in the organ of Corti. Acta Otolaryngol (Stockh) Suppl 467: 189–193.

Khanna SM, Ulfendahl M, Flock Å (1989d). Dependence of cellular responses on signal level. Acta Otolaryngol (Stockh) Suppl 467: 195–203.

Khanna SM, Ulfendahl M, Flock Å (1989e). Tuning of harmonic components in cellular mechanical responses. Acta Otolaryngol (Stockh) Suppl 467: 205–208.

Lund DT, Khanna SM (1989). A digital system for the generation of acoustic stimuli and the analysis of cellular vibration data. Acta Otolaryngol (Stockh) Suppl 467: 77–89.

Teich MC, Keilson SE, Khanna SM (1989a). Rectification models in cochlear transduction. Acta Otolaryngol (Stockh) Suppl 467: 235–240.

Teich MC, Keilson SE, Khanna SM (1989b). Models of nonlinear vibration II. Oscillator with bilinear stiffness. Acta Otolaryngol (Stockh) Suppl 467: 249–256.

Willemin JF, Khanna SM, Dändliker R (1989). Heterodyne interferometer for cellular vibration measurement. Acta Otolaryngol (Stockh) Suppl 467: 35–42.